

1 Helm Glacier projected to vanish within a decade

2 Jeffrey W. CROMPTON¹, Brian MENOUNOS^{1,3,4}, Mark EDNIE²

3 ¹*Geological Survey of Canada, Natural Resources Canada, Vancouver, British Columbia, Canada*

4 ²*Geological Survey of Canada, Natural Resources Canada, Ottawa, ON, Canada,*

5 ³*Department of Geography, Earth, and Environmental Science, University of Northern British Columbia,*
6 *Prince George, British Columbia, Canada*

7 ⁴*Hakai Institute, Campbell River, British Columbia, Canada*

8 **ABSTRACT.** Helm Glacier is one of four glaciers in Canada with a mass
9 balance record which exceeds 40 years. This World Glacier Monitoring Service
10 reference glacier is strongly out of balance with present day climate. An ice
11 penetrating radar survey reveals a mean and maximum ice thickness of 13 and
12 35 m respectively. We combine ice thickness data and altimetric data from
13 repeat lidar surveys to project ice disappearance using simple extrapolation
14 and a regression model which predicts surface elevation change based on
15 incoming shortwave radiation, winter snow accumulation, positive degree days,
16 slope and aspect. Both approaches project the disappearance of Helm Glacier
17 by 2035. From a sensitivity analysis we estimate that Helm Glacier is over
18 5 °C away from its equilibrium mass balance, consistent with the observed
19 temperature change over the period 1950 to present.

20 INTRODUCTION

21 Over the last four years, glaciers in Western Canada and the conterminous US lost twice as much mass
22 as during the period 2010-2019 (Menounos and others, 2025). This mass loss occurred primarily through
23 widespread surface thinning driven by warm, dry conditions and general darkening of glacier surfaces. In
24 terms of surface area, Canada contains about 185,000 km² of glacierized terrain, about one quarter of the
25 global total (Consortium, 2023). Given the importance of glacier runoff to Canada's economy, the federal

26 government established a network of glacier monitoring sites during the International Hydrological Decade
27 (Ommannay, 1986). These sites became operational in 1965 and, ten years later, the Government of Canada
28 added Helm Glacier to its list of monitoring sites given its maritime environment Ommannay and others
29 (2002). Helm Glacier is a World Glacier Monitoring Service (WGMS) reference glacier and only one of
30 four glaciers in Canada where mass balance observations exceed 40 years. In addition to their importance
31 of recording seasonal-to-annual response of glaciers to climate change, *in situ* glacier monitoring records
32 provides seasonal-to-annual observations required for regional upscaling of glacier mass change (Zemp and
33 others, 2019). The objectives of this short note are to describe recent changes of Helm Glacier and estimate
34 when Helm Glacier is projected to disappear.

35 STUDY AREA AND METHODS

36 Helm Glacier ($49^{\circ}57'29''$ N, $122^{\circ}59'13''$ W) lies on the western edge of Garibaldi Provincial Park in the
37 Pacific Ranges of the southern Coast Mountains in the traditional territory of the Squamish Nation (Figure
38 1). The small (0.4 km^2) glacier's elevation range is from 1780 m a.s.l. to 2150 m a.s.l.

39 Glacier mapping and mass balance surveys

40 We digitized the extent of Helm Glacier from end-of-summer spaceborne (Landsat 5,7,8,9) and airborne
41 ortho-imagery, the latter acquired by the Hakai-UNBC Airborne Coastal Observatory (Donahue and others,
42 2023). We take the product of the ground sampling distance of the imagery and the glacier's perimeter to
43 reflect the uncertainty in our mapping. As described above, Helm Glacier represents a WGMS reference
44 glacier where mass balance measurements follow the stratigraphic method (Kaser and others, 2003). The
45 glacier's seasonal balance is derived from 6-8 ablation stakes positioned along the centreline of the glacier,
46 snow depth probing and end-of-winter snow pits where snow density and stratigraphic observations are
47 made. Those data are used to generate seasonal and annual mass balance for the glacier and by updating
48 the glacier area every few years.

49 Ice-penetrating radar

50 We completed an ice-penetrating radar survey of Helm Glacier on 21 May, 2025. The Blue Systems
51 Integration Ltd. radar system uses resistively-loaded dipole antennas with a centre frequency of 10 MHz,
52 has 12-bit resolution and yields a sampling rate of up to 250 Megasamples per second (Mingo and Flowers,
53 2010). The radar system contains a single frequency GNSS system with an accuracy of ± 5 m. To increase
54 the vertical accuracy for the glacier surface (± 0.5 m), we acquired airborne Lidar for the surface elevation

55 of the glacier on 24 April, 2025. Details about methods used for Lidar acquisition can be found elsewhere
56 (Menounos and others, 2025). Observations of surface elevation change from a sonic depth ranger equipped
57 with satellite telemetry Bevington and others (2025), reveals about 1 m of thinning between our Lidar and
58 radar surveys. We processed the radar data with IceRadarAnalyzer 6.3.1, with an antenna spacing of 15 m
59 and assuming a velocity through ice at 1.68×10^8 m s⁻¹ (Reynolds, 2011). To increase the signal-to-noise
60 ratio of the data, we averaged 128 stacks for each trace in the radargram and then applied gain and filtering
61 for identification of bed reflectors. We completed crossover analysis (i.e. where two radar transects overlap)
62 and propagated in quadrature the uncertainty using one-quarter of the radar wavelength Reynolds (2011)
63 and uncertainty that arises from surface slope to yield an error of ice thickness of ± 4.5 m. 2D linear
64 interpolation of the ice thickness data yielded a map of ice thickness (10 m ground sampling distance -
65 GSD).

66 Projection of glacier disappearance

67 We use an area of 0.01 km² to define the threshold at which point Helm Glacier would cease to exist.
68 To estimate the year when this will occur, we forward model the yearly surface elevation change of Helm
69 Glacier using two approaches described below. Both of these approaches use surface elevation data obtained
70 from repeat Lidar surveys of Helm Glacier completed at the end of ablation season in 2020–2024. These five
71 autumn surveys provide elevation change maps for 2021, 2022, 2023 and 2024, and those airborne surveys
72 followed the same methods described in Menounos and others (2025). Elevation change at a given point can
73 be equated to annual surface mass balance given the thinness of the glacier (i.e. negligible ice dynamics)
74 and minimal extent of retained snow on the glacier (i.e. density-to-mass conversion is simplified). The
75 elevation change maps are downsampled to 10 m GSD to match the ice thickness grid. Co-registration of
76 elevation change maps used methods described in Nuth and Kääb (2011) and Hugonet and others (2022)
77 available in the XDEM package (<https://pypi.org/project/xdem/>).

78 Our first approach (method 1) averages the surface elevation change at each grid cell over the four year
79 period, then simply differences this average elevation change from the ice thickness grid each year. Ice
80 vanishes at a given grid cell when the total melt exceeds the ice thickness of the column. The error in area
81 is simply taken by recomputing the elevation change within the ice thickness error bounds of ± 4.5 m.

82 For the second approach (method 2), we use a regression model to predict elevation change \mathbf{dh}^y based
83 on the design matrix of observations \mathbf{X}^y for each of the years $j = \{2021, 2022, 2023, 2024\}$ for each of the
84 n grid cells (method 2). Linear regression can be used to model mass change at the regional (Lliboutry,

85 1974; Anilkumar and others, 2023; Reynaud and others, 1986) to individual ablation stake scale (Zekollari
 86 and Huybrechts, 2018). The matrix \mathbf{X}^y is composed of slope ($\boldsymbol{\theta}^y$), orientation ($\boldsymbol{\alpha}^y$), positive-degree days
 87 (\mathbf{PDD}^y), shortwave radiation at the surface ($\mathbf{SW}_{\downarrow}^y$) and snow depth (\mathbf{h}^y). The regression $\mathbf{dh} = \mathbf{X}\boldsymbol{\beta} + \boldsymbol{\varepsilon}$
 88 is computed on the matrix \mathbf{X} and observations \mathbf{dh} that are concatenated across the four-year record. The
 89 optimal coefficients are estimated through least-squares regression as, $\hat{\boldsymbol{\beta}} = (\mathbf{X}^T \mathbf{X})^{-1} \mathbf{X}^T \mathbf{M}$. The model is
 90 validated by modelling the surface change for each year individually as $\hat{\mathbf{M}}^j = \mathbf{X}^j \hat{\boldsymbol{\beta}}$, with the R^2 computed
 91 between the yearly difference in observed and modelled elevation change at each grid cell.

92 Computed PDDs are summed in the time intervals given by the LiDAR acquisition dates as $\mathbf{PDD}^y =$
 93 $\frac{1}{24} \sum T(z)$ for $T > 0^\circ\text{C}$. The temperature (T) is taken from dynamically downscaled hourly ERA-5 land
 94 temperatures (Hersbach and others, 2020) given at the nearest grid point and lapsed up from 1550 m to
 95 the elevation of each grid cell. Similar to the melt-season lapse rate computed by Shea and others (2009)
 96 of $-6.0^\circ\text{C km}^{-1}$, we calculate April to October lapse rates from a series of nearby weather stations as -
 97 $5.8^\circ\text{C km}^{-1}$. We compute annual snow depth for the glacier using snow depth collected each April at the
 98 stake locations which yields a relation between snow depth and elevation. Summer (May-Sept) incoming
 99 shortwave radiation is computed my multiplying a shading factor matrix computed in the HORAYZON
 100 v1.2 model (Steger and others, 2022) with the mean of the daily averaged downwelling shortwave radiation
 101 obtained from the nearest gridpoint of ERA5-Land reanalysis. Although the shading model and surface
 102 normal shortwave radiation both depend on surface slope and aspect, we include slope and aspect as
 103 individual columns in the design matrix to capture other mass balance processes like snow redistribution.

104 To forward model the ice loss, we start with the 2024 DEM and force the model with the average of the
 105 PDD fields from 2014 to 2024, all computed at the 2024 grid cell elevations from April 01 to October 31.
 106 The forcing for \mathbf{SW}_{\downarrow} and the snow depth field \mathbf{h} field are generated from averaging the 2020–2024 fields
 107 used in the regression model. At each step forward in time, we recompute the surface elevation, slope,
 108 aspect, \mathbf{PDD} and snow-depth fields, but keep \mathbf{SW}_{\downarrow} fixed in time. We estimate uncertainty in elevation
 109 change by initializing the ice thickness at the ± 4.5 m error bounds and by varying the lapse rate by $\pm 5\%$.

110 Mass balance sensitivity

111 We test the net mass balance (b_n) sensitivity of our model to changes in temperature as $C_T = \frac{\partial b_n}{\partial T}$ and
 112 precipitation as $C_P = \frac{\partial b_n}{\partial P}$ by varying the mean summer temperature and the mean winter accumulation
 113 of the model (e.g. Cuffey and Paterson, 2010). Numerical derivatives for C_T and C_P are computed for
 114 the current temperature and accumulation conditions. We test the sensitivity of: i) yearly specific mass

balance using the 2024 reference surface (e.g. Elsberg and others, 2001); and ii) integrated mass balance by allowing the accumulation area to grow from the 2024 reference surface. In the forward model for sensitivity, PDDs are calculated at each grid cell for each incremental temperature change, whereas changes in winter accumulation are input directly into the regression equation. To convert elevation change to mass loss (m w.e.), cells with negative elevation change are multiplied by an elevation-to-mass conversion factor of 0.917. Positive elevation changes indicative of snow accumulation are multiplied by a factor of 0.41, which we derive from the integrated snow pit density averaged from up to two pit locations per year since 1997. We compute the percent change in temperature from the mean ERA5-Land summer temperature at the mean elevation of the glacier from 2014–2024. The percent change in accumulation is computed by normalizing the offset in accumulation by the glacier-wide average snow depth field used in the forward model. We compare our modelled temperature sensitivities to observed sensitivities at Helm Glacier, computed as the slope of the regression between ERA5-Land mean summer temperature and net specific mass balance from 1975 to 2024 from glaciological mass balance data (WGMS, 2024).

128 Mass balance sensitivity

We test the net mass balance (b_n) sensitivity of our model to changes in temperature as $C_T = \partial b_n / \partial T$ and precipitation as $C_P = \partial b_n / \partial P$. Sensitivities are computed by varying the mean summer temperature and the mean winter accumulation of the model (e.g. Cuffey and Paterson, 2010). Numerical derivatives for C_T and C_P are computed for the current temperature and accumulation conditions. We test the sensitivity of i) yearly specific mass balance using the 2024 reference surface (e.g. Elsberg and others, 2001) and ii) integrated mass balance by allowing the accumulation area to grow from the 2024 reference surface. In the forward model for sensitivity, PDDs are calculated at each grid cell for each incremental temperature change, whereas changes in winter accumulation are input directly into the regression equation. To convert elevation change to mass loss in m w.e., cells with negative elevation change are multiplied by an ice density factor of 0.917. Positive elevation changes indicative of snow accumulation are multiplied by a density factor of 0.41, which is the integrated snow pit density averaged from up to two pit locations per year from 14 years of spring surveys dating back to 1997. We compute the percent change in temperature by normalizing by the mean ERA5-Land summer temperature at the mean elevation of the glacier from 2014–2024. The percent change in accumulation is computed by normalizing the offset in accumulation by the glacier-wide average snow depth field used in the forward model. We compare our modelled temperature sensitivities to observed sensitivities at Helm Glacier, computed as the slope of the regression between ERA5-Land mean

145 summer temperature and net specific mass balance from 1975 to 2024 from glaciological mass balance data
146 (WGMS, 2024).

147 RESULTS

148 Helm Glacier reached its maximum Holocene extent (4.5 km^2) at about 1690-1710 CE (Koch and others,
149 2009). Except for period of slowed recession with a minor advance between the late 1960's and 1970's,
150 Helm Glacier experienced widespread thinning with attendant shrinkage throughout the Twentieth Century
151 (Koch and others, 2009). Between 1928 and 2024, Helm Glacier lost about 90 % of its surface area with
152 notable accelerated area loss after 2015 (Figure 2). Pronounced retreat and thinning over the last eight
153 years led to fragmentation of the glacier in its uppermost elevations. Marginal retreat along the glacier's
154 mid section will split the lower and upper portions of the glacier within a year or two (Figure 1).

155 Since 1975, Helm Glacier experienced only five years of positive mass balance (WGMS, 2024). Recent
156 imagery of the glacier reveals widespread loss of firn with negligible accumulation area especially over the
157 last four years. Glaciological mass balance data averaged over the past seven years show an annual balance at
158 the terminus of -3.6 m w.e. and -1.6 m w.e. at the summit. During that time period, the yearly accumulation
159 averaged over the entire glacier was 1.85 m w.e. From 1984 to present, Helm Glacier experienced the most
160 negative mass balance of all 16 WGMS monitored glaciers in North America (WGMS, 2024). Helm Glacier
161 experienced its most extreme year of mass loss in 2023 (-4.34 m w.e.), roughly 2.5 times greater than the
162 average of the previous six years. Many glacier in western Canada and the Conterminous US (RGI region
163 02) experienced pronounced glacier mass loss driven in part by warm, dry conditions (Menounos and others,
164 2025).

165 In addition to climate, changes in glacier area through time is also influenced by underlying terrain as
166 exemplified by the rapid drop in area in the late 1980s as thin ice in the upper basin vanishes (Fig. 2).
167 Regional trends in accelerated area and mass loss around 2010 (Bevington and Menounos, 2022; Menounos
168 and others, 2019) and again in 2020 (Menounos and others, 2025) cannot be easily distinguished at Helm,
169 though Helm Glacier undergoes accelerating area loss that continues from 2014 to present, which does not
170 appear to be controlled by the basin geometry.

171 From the ice-penetrating radar survey we observe that the remaining ice at Helm Glacier is thin, with
172 an average thickness of 13 m and a maximum thickness of 35 m. Our projections of surface elevation
173 change indicate that Helm Glacier will vanish within a decade (Figs. 2 and 3). Helm Glacier is forecast to
174 decrease into fragmented patches of less than 0.1 km^2 by 2028 ± 0.5 (method 1) or by 2029 ± 0.5 (method

175 2). Projected area loss patterns are controlled predominately by the remaining ice thickness rather than
 176 elevation, orientation and slope. For the linear regression, the R^2 is 0.83 and $\hat{\beta}$ values are all statistically
 177 significant with $p < 0.001$, with the exception of $\hat{\beta}$ for \mathbf{SW}_\downarrow at $p = 0.065$. Given that slope and aspect
 178 account for the greatest spatial variation in incoming shortwave radiation, omitting the \mathbf{SW}_\downarrow and snow
 179 accumulation fields from the design matrix can lead to model fits for the 2020–2021 and 2023–2024 melt
 180 years with $R^2 \sim 0.7$. However, the reanalysis masked shortwave data are needed to adequately model the
 181 high melt season of 2022–2023. Similarly, the design matrix needs to include snow accumulation data to
 182 adequately fit the high snow accumulation season of 2021–2022. Relative to the uncertainty in ice depth,
 183 the regression model shows little sensitivity to a variation in lapse rate of $\pm 5\%$.

184 Calculating the specific balance from the 2024 reference surface shows that a net-zero balance can be
 185 achieved with an increase in precipitation of 1.5 m w.e. (36% mean winter snow accumulation) at the current
 186 temperature, or a change in temperature of -6.8°C (95% mean winter snow accumulation) at the current
 187 accumulation (Fig. 4 a). By allowing the accumulation area to grow, we compute a volumetric balance
 188 sensitivity that is slightly more optimistic (Fig. 4 b), requiring an increase in precipitation of 1.1 m w.e.
 189 (28%) at the current temperature, or a change in temperature of -5.1°C (71%).

190 For current conditions at Helm Glacier, we compute a sensitivity to temperature as
 191 $C_T = -0.65 \text{ m w.e. yr}^{-1} \text{ }^\circ\text{C}^{-1}$ while the sensitivity to accumulation is $C_P = 0.97 \text{ m w.e. yr}^{-1} \text{ m w.e.}^{-1}$.
 192 On a unit-by-unit basis, the glacier is therefore 1.5 times more sensitive to changes in winter accumulation
 193 relative to changes in mean summer temperature. However, comparing the sensitivities by percentage
 194 change yield $C_P/C_T = 0.84$. The mass balance sensitivities for both the volumetric and specific mass
 195 balance methods yield very similar results. Our modelled value of $C_T = -0.65 \text{ m w.e. yr}^{-1} \text{ }^\circ\text{C}^{-1}$ is in
 196 agreement to the observed mass balance temperature sensitivity of $C_T = -0.64 \text{ m w.e. yr}^{-1} \text{ }^\circ\text{C}^{-1}$.

197 DISCUSSION

198 Both methods used to project the demise of Helm Glacier indicate that survival of the glacier beyond the
 199 next decade is unlikely. Extrapolating the average elevation change forward in time (method 1) is more
 200 conservative than the regression model (method 2) because surface parameters like slope, orientation and
 201 elevation that are updated at each yearly time step in the regression model create a positive feedback in
 202 melt rate, which is not captured with the simple extrapolation. Several intricacies complicate the projected
 203 disappearance of Helm Glacier. For each melt season, modelled surface elevation change is underestimated
 204 along the glacier's eastern margin where avalanche accumulation and shading occurs. Elevation change is

205 overestimated at the eastern head of the glacier where snow redistribution by wind causes a reversal of the
206 accumulation gradient. Linearly interpolating and extrapolating snow depth measurements to the snow
207 depth field yields the best R^2 averaged across all observation periods, but in cases of extreme years for
208 snow redistribution, a second or third-order polynomial fit can significantly increase the fit at high and low
209 elevations for that year. Given that this thin glacier is strongly out of balance with present-day climate,
210 capturing these finer-scale patterns of accumulation and melt would not change the fate of Helm Glacier's
211 extinction within the decade, however.

212 The linear regression model is driven by average temperatures over the past decade and an average snow
213 accumulation field. As such, the forward model does not capture extreme melt events observed regionally
214 and at Helm Glacier. Examples of events and processes that likely make our projections conservative
215 include the intense melt year of 2023 (Menounos and others, 2025), an equilibrium-line elevation that is
216 starting to rise above the head of the glacier (Bevington and Menounos, 2025), surface darkening from
217 wildfire ash deposition that decreases ice albedo (Menounos and others, 2025; Aubry-Wake and others,
218 2022) and proglacial lake development leading to basal melt and calving (Carrivick and Tweed, 2013;
219 Shugar and others, 2020). These processes that we do not account for should lead to an overestimate of the
220 cooling required to reach equilibrium mass balance (see Fig. 4). However, the temperature shifts that we
221 derive in the sensitivity analyses are consistent with the observed increase in mean summer temperature of
222 4.6°C from 1950 to present at the nearest ERA5-Land grid point. Winter balance data from Helm Glacier
223 over the monitoring period shows no evidence of changes in precipitation that could explain the glacier's
224 disequilibrium.

225 CONCLUSION

226 Over the last 97 years, Helm Glacier lost 90% of its surface area, with notable accelerated area and
227 mass loss over the past decade. We estimate that Helm Glacier is over 5°C away from equilibrium mass
228 balance conditions under the present-day pattern of winter accumulation. The magnitude of disequilibrium
229 is consistent with an increase in mean summer temperature of roughly 5°C from over the last 75 years.
230 These conditions coupled with its thinness implies that the glacier will vanish within the next decade. While
231 the volume of water storage in Helm Glacier is small, the loss of this glacier will reduce the availability
232 of long-term *in situ* mass balance observations from North America which are essential for improving
233 physically-based models of glacier change.

234 ACKNOWLEDGEMENTS

235 We are grateful for the research supported from the National Sciences and Engineering Research Council of
236 Canada, Tula Foundation and Natural Hazards and Climate Change Geoscience Program at the Geological
237 Survey of Canada. We appreciate the site access granted by B.C. Parks. The ice radar survey was made
238 possible by the help of Felix Parkinson while mass balance monitoring was made possible with the help of
239 Jason VanderSchoot.

240 AUTHOR CONTRIBUTIONS

241 Jeff and Brian co-wrote the manuscript. Brian provided the reanalysis and LiDAR data. Mark collected all
242 *In situ* mass balance observations from 2019 to present and Brian and Mark mapped historic area change.
243 Jeff collected and processed the radar data and performed the regression analysis.

244 DATA AND CODE AVAILABILITY

245 All code and data used for the regression analysis can be obtained from
246 https://github.com/jwheelsc/helm_SEC

247 REFERENCES

- 248 Anilkumar R, Bharti R, Chutia D and Aggarwal SP (2023) Modelling point mass balance for the glaciers of the
249 Central European Alps using machine learning techniques. *The Cryosphere*, **17**(7), 2811–2828
- 250 Aubry-Wake C, Bertoncini A and Pomeroy JW (2022) Fire and ice: The impact of wildfire-affected albedo and
251 irradiance on glacier melt. *Earth's Future*, **10**(4), e2022EF002685
- 252 Bevington AR and Menounos B (2022) Accelerated change in the glaciated environments of western Canada revealed
253 through trend analysis of optical satellite imagery. *Remote Sensing of Environment*, **270**, 112862
- 254 Bevington AR and Menounos B (2025) Glaciers in western North America experience exceptional transient snowline
255 rise over satellite era. *Environmental Research Letters*, **20**(5), 054044
- 256 Bevington AR, Menounos B and Ednie M (2025) Satellite telemetry of surface ablation observations to inform spatial
257 melt modelling, Place Glacier, British Columbia, Canada. *EGUsphere*, **2025**, 1–30
- 258 Carrivick JL and Tweed FS (2013) Proglacial lakes: character, behaviour and geological importance. *Quaternary
259 Science Reviews*, **78**, 34–52
- 260 Consortium R (2023) Randolph glacier inventory-a dataset of global glacier outlines, version 7. *NASA National Snow
261 and Ice Data Center Distributed Active Archive Center (DAAC) data set*, F6JMOVY5NAVZ

- 262 Cuffey KM and Paterson WSB (2010) *The physics of glaciers*. Academic Press
- 263 Donahue CP, Menounos B, Viner N, Skiles SM, Beffort S, Denouden T, Arriola SG, White R and
264 Heathfield D (2023) Bridging the gap between airborne and spaceborne imaging spectroscopy for mountain
265 glacier surface property retrievals. *Remote Sensing of Environment*, **299**, 113849, ISSN 0034-4257 (doi:
266 <https://doi.org/10.1016/j.rse.2023.113849>)
- 267 Elsberg D, Harrison W, Echelmeyer K and Krimmel R (2001) Quantifying the effects of climate and surface change
268 on glacier mass balance. *Journal of Glaciology*, **47**(159), 649–658
- 269 Hersbach H, Bell B, Berrisford P, Hirahara S, Horányi A, Muñoz-Sabater J, Nicolas J, Peubey C, Radu R, Schepers
270 D and others (2020) The ERA5 global reanalysis. *Quarterly journal of the royal meteorological society*, **146**(730),
271 1999–2049
- 272 Hugonnet R, Brun F, Berthier E, Dehecq A, Mannerfelt ES, Eckert N and Farinotti D (2022) Uncertainty analysis
273 of digital elevation models by spatial inference from stable terrain. *IEEE Journal of Selected Topics in Applied
274 Earth Observations and Remote Sensing*, **15**, 6456–6472
- 275 Kaser G, Fountain A and Jansson P (2003) *A Manual for Monitoring the Mass Balance of Mountain Glaciers*.
276 UNESCO, Paris
- 277 Koch J, Menounos B and Clague JJ (2009) Glacier change in Garibaldi Provincial Park, southern Coast Mountains,
278 British Columbia, since the Little Ice Age. *Global and Planetary Change*, **66**(3-4), 161–178
- 279 Lliboutry L (1974) Multivariate statistical analysis of glacier annual balances. *Journal of Glaciology*, **13**(69), 371–392
- 280 Menounos B, Hugonnet R, Shean D, Gardner A, Howat I, Berthier E, Pelto B, Tennant C, Shea J, Noh MJ and
281 others (2019) Heterogeneous changes in western North American glaciers linked to decadal variability in zonal
282 wind strength. *Geophysical Research Letters*, **46**(1), 200–209
- 283 Menounos B, Huss M, Marshall S, Ednie M, Florentine C and Hartl L (2025) Glaciers in Western Canada-
284 conterminous US and Switzerland experience unprecedented mass loss over the last four years (2021–2024).
285 *Geophysical Research Letters*, **52**(12), e2025GL115235
- 286 Mingo L and Flowers GE (2010) An integrated lightweight ice-penetrating radar system. *Journal of Glaciology*,
287 **56**(198), 709–714
- 288 Nuth C and Kääb A (2011) Co-registration and bias corrections of satellite elevation data sets for quantifying glacier
289 thickness change. *The Cryosphere*, **5**(1), 271–290
- 290 Ommann C (1986) Mapping Canada's glaciers since 1965. *Annals of glaciology*, **8**, 132–134
- 291 Ommann C, Demuth M and Meier M (2002) Glaciers of North America. *US Geological Survey Professional Paper*,
292 **1386**, 23
- 293 Reynaud L, Vallon M and Letreguilly A (1986) Mass-balance measurements: problems and two new methods of
294 determining variations. *Journal of Glaciology*, **32**(112), 446–454

- 295 Reynolds JM (2011) *An introduction to applied and environmental geophysics*. John Wiley & Sons
- 296 Shea JM, Moore RD and Stahl K (2009) Derivation of melt factors from glacier mass-balance records in western
297 Canada. *Journal of Glaciology*, **55**(189), 123–130
- 298 Shugar DH, Burr A, Haritashya UK, Kargel JS, Watson CS, Kennedy MC, Bevington AR, Betts RA, Harrison S and
299 Stratman K (2020) Rapid worldwide growth of glacial lakes since 1990. *Nature climate change*, **10**(10), 939–945
- 300 Steger CR, Steger B and Schär C (2022) HORAYZON v1. 2: an efficient and flexible ray-tracing algorithm to compute
301 horizon and sky view factor. *Geoscientific Model Development*, **15**(17), 6817–6840
- 302 WGMS (2024) Fluctuations of glaciers database. World Glacier Monitoring Service, Zurich, Switzerland. (doi:
303 10.5904/wgms-fog-2024-07)
- 304 Zekollari H and Huybrechts P (2018) Statistical modelling of the surface mass-balance variability of the Morteratsch
305 glacier, Switzerland: strong control of early melting season meteorological conditions. *Journal of Glaciology*,
306 **64**(244), 275–288
- 307 Zemp M, Huss M, Thibert E, Eckert N, McNabb R, Huber J, Barandun M, Machguth H, Nussbaumer SU, Gärtner-
308 Roer I, Thomson L, Paul F, Maussion F, Kutuzov S and Cogley JG (2019) Global glacier mass changes and their
309 contributions to sea-level rise from 1961 to 2016. *Nature*, **568**(7752), 382–386

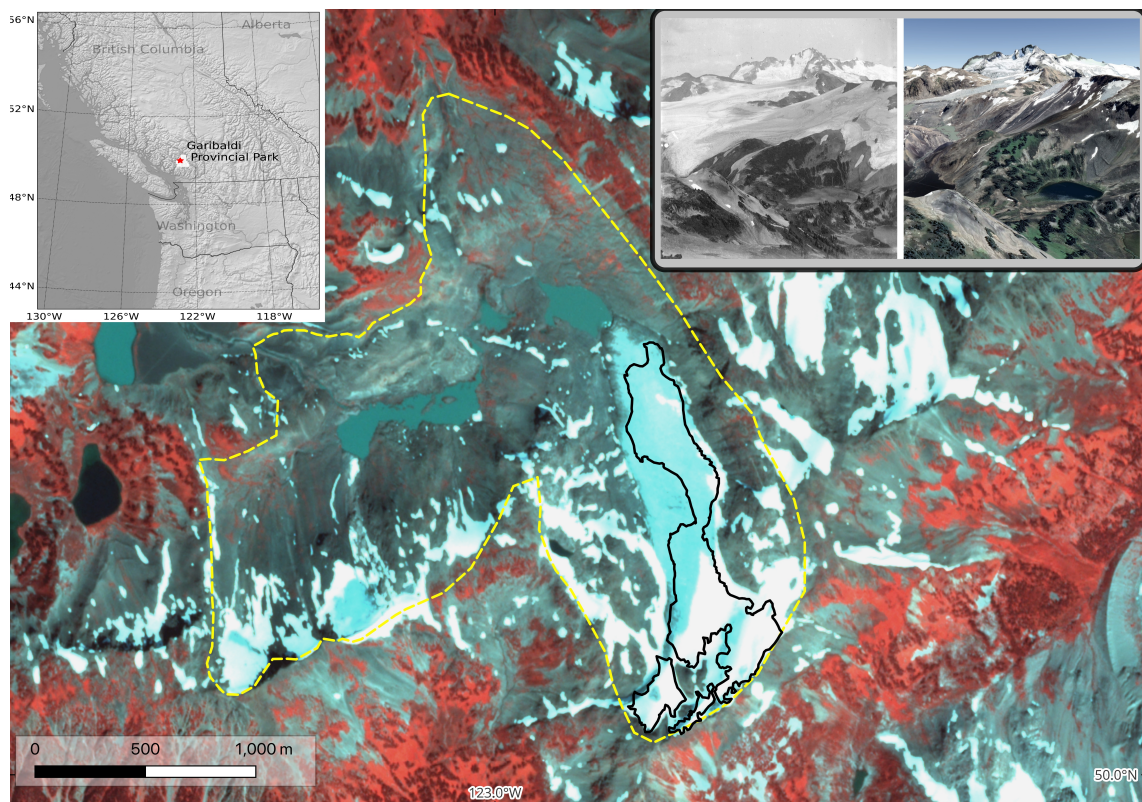


Fig. 1. **Inset map:** Helm Glacier (red star) within Garibaldi Provincial Park. **Background image:** PlaceScope color composite (NIR-R-G) of Helm Glacier [28 August, 2017] and surrounding terrain. Black solid and yellow dashed lines respectively denote glacier extent in 2024 and 1928 survey photo-topographic survey of the glacier (Koch and others, 2009). **Upper right images:** Oblique image (left) of Helm Glacier in 1910s (unknown photographer) and glacier extent from Google Earth Engine (6 Aug, 2019 imagery). 1910s image courtesy of City of Vancouver Archives.

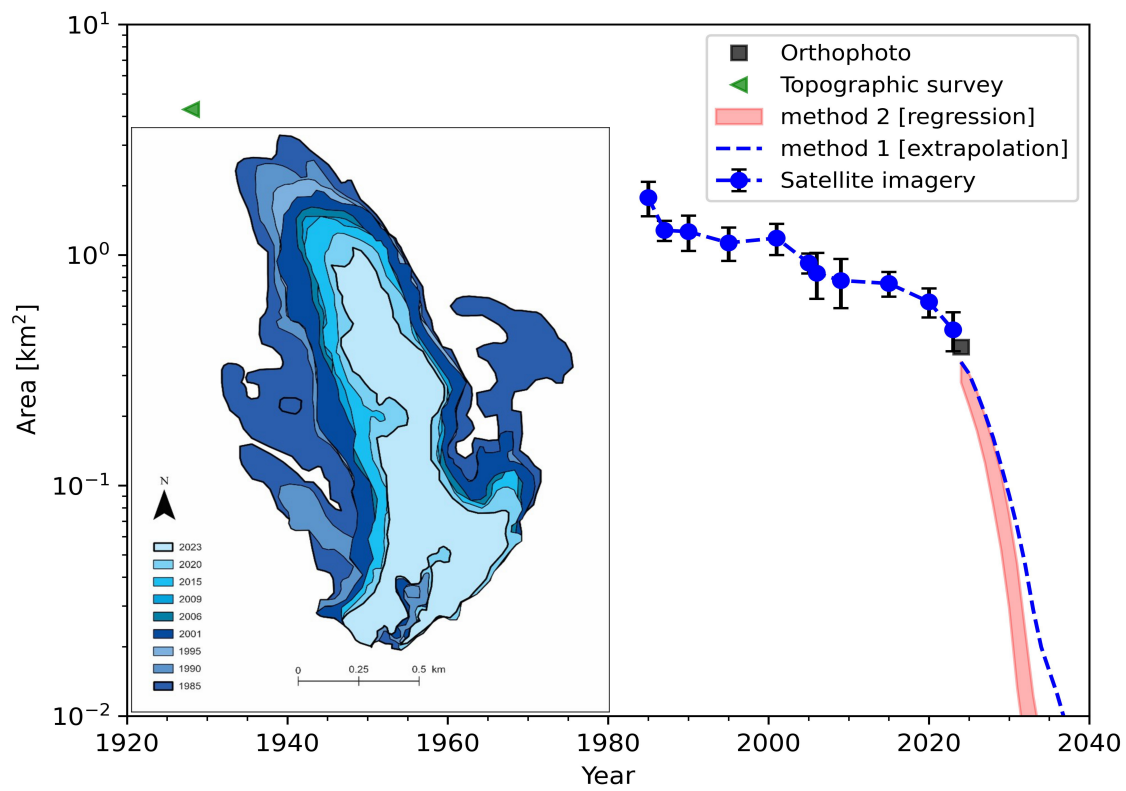


Fig. 2. Modelled and observed glacier area change through time. Error bars denote mapping uncertainty. Pink shading reflects the uncertainty range for the regression model obtained by initializing the model with the error bounds on ice thickness. Error bounds for the elevation change extrapolation are not shown, but are similar in spread to the regression uncertainty. **Inset figure:** Planimetric change of Helm Glacier from Satellite imagery

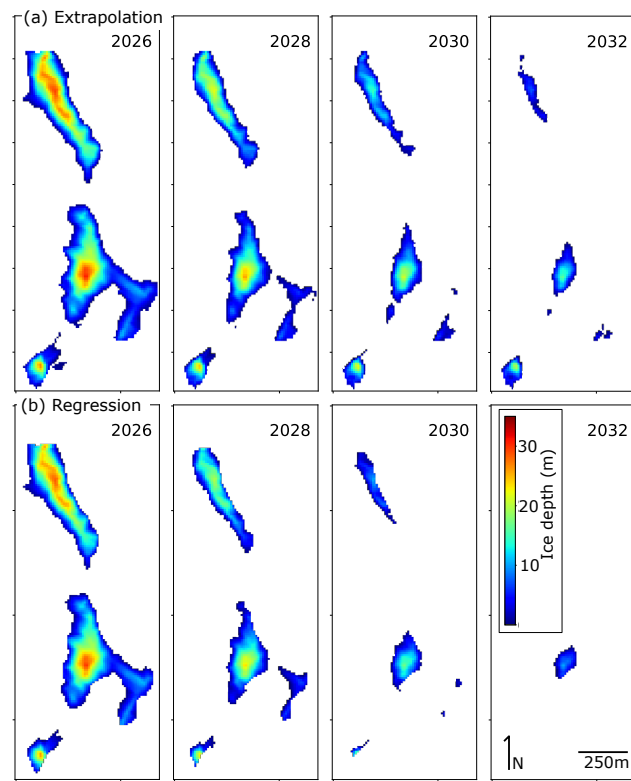


Fig. 3. (a - top panels) Forward model of glacier area and thickness by extrapolation of mean elevation change field between 2020 and 2024 (method 1) and (b - bottom panels) multivariate linear regression (method 2).

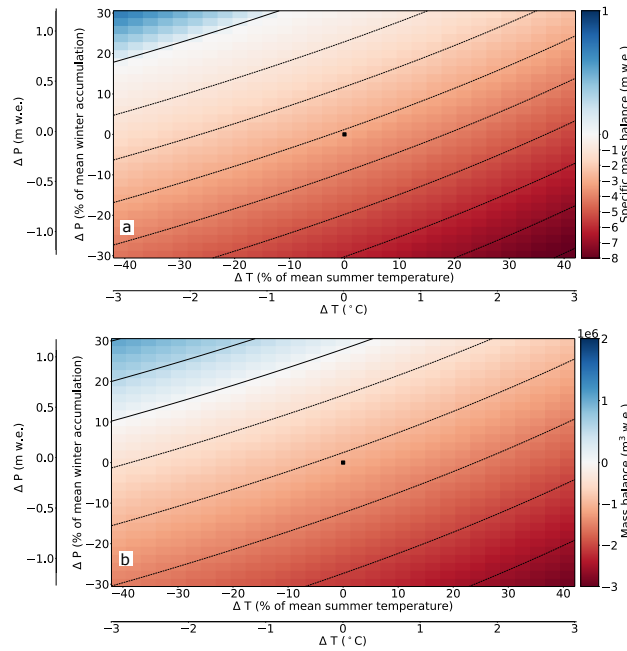


Fig. 4. Mass balance as function of absolute changes in temperature and accumulation with secondary axes mapped onto percent variation in mean summer temperature and winter accumulation, respectively. (a) Specific mass balance computed from 2024 reference surface with contour intervals of 1 m w.e. (net zero separating blue and red). (b) Volumetric mass balance computed by allowing the accumulation area to grow where mass balance is positive (contour intervals of 1×10^6 m³ w.e.) Black dots show reference state for current conditions.